Batteries & Supercaps

Research Article
doi.org/10.1002/batt.202500305

Chemistry Europe
European Chemical Societies Publishing

www.batteries-supercaps.org

Preintercalation Induced Transition from Double Layer to Redox Calcium-Ion Storage in Vanadium Carbide MXene

Suman Yadav and Narendra Kurra*

MXenes are a versatile class of two-dimensional (2D) materials that exhibit proton-induced pseudocapacitance, however, intercalation capacitive behavior in neutral electrolytes limits the charge storage capacities. In this work, the design of pseudocapacitive vanadium carbide (V_2CT_x) MXene electrodes in calcium-ion electrolytes is reported. By incorporation of room temperature ionic liquid, 1-ethyl-3-methylimidazolium bis(trifluoromethanesulfonyl)imide (EMIM-TFSI), as a preintercalant, a transition from electrical double layer to redox charge storage is observed. Facile diffusion of high charge density Ca-ions to inaccessible surface-active sites is enabled by the confined fluid effect of ionic liquid, results in a specific calciation capacity of 116 mAh g^{-1} at a current density of 0.05 A g^{-1}. However, inevitable capacity loss limits the long-term stability, which is possibly due to spontaneous intercalation of water leading to plausible (electro)chemical dissolution of V_2CT_x MXene in aqueous Ca-ion electrolyte as confirmed by in situ X-ray diffraction studies. By the optimal choice of a hybrid electrolyte consisting of propylene carbonate and water, the charge storage capacity is improved up to 180 mAh g^{-1} at a current density of 0.09 A g^{-1} with an enlarged potential window of 1.6 V and capacity retention of 70% over 2000 cycles. This study opens avenues for exploring hybrid electrolytes toward long-term cycling stability of MXene electrodes.

1. Introduction

Pseudocapacitive energy storage bridges the capacitive and Faradaic classes of charge storage while offering simultaneous high charge capacities at high rates.[1] Two dimensional (2D) transition metal carbides, nitrides, and carbonitrides–popularly known as MXenes–are a fascinating class of high rate-charge storage materials due to a unique combination of metallic conductivity and transition metal oxide/hydroxide-like redox chemistry.[2,3] The top-down aqueous wet chemical etching method introduces the inherent surface functional groups such as —OH, =O, —F, and —Cl, rendering MXenes to be hydrophilic.[4] By virtue of intrinsic hydrophilicity, MXenes are known to intercalate aqueous cations spontaneously across their interlayer spaces.[5] For instance, titanium carbide ($Ti_3C_2T_x$) MXene exhibits proton-induced pseudocapacitive behavior due to the protonation of redox-active Ti-O groups.[6] However, the charge storage capacities of MXenes are limited by the formation of electrical double layers (EDLs) in the case of neutral and organic electrolytes.[7] By virtue of multiple oxidation states of vanadium, V_2CT_x MXene has become a versatile redox charge storage host and, indeed, the second most widely explored electrode material (MXene) after $Ti_3C_2T_x$ for energy storage applications.[8] Furthermore, vanadium has an intriguing electrochemistry that has been underexplored due to its chemical instability. However, recent progress in the synthesis protocols has improved chemical stability of V_2CT_x MXene to significant extent.[9] Fundamental electrochemical studies confirmed the pseudocapacitance of V_2CT_x MXene in acidic and basic electrolytes, giving rise to capacitance up to 386 F g^{-1} in 1M LiOH electrolytes.[10] Due to the limited cycling stability of the V_2CT_x MXene electrodes in aqueous medium, research efforts were diverted toward employing non-aqueous electrolytes.

Driven by the urgent need for development of post Li-ion chemistries, V_2CT_x MXene was employed as a cathode for the design of sodium-ion hybrid capacitors while using hard carbon as an anode.[11] Interestingly, V_2CT_x was also employed as a cathode for Al-batteries with a specific capacity of 165 mAh g^{-1} at a current density of 100 mA g^{-1}.[12] V_2CT_x MXene also showed pseudocapacitance in aqueous ammonium acetate electrolytes, delivering a specific capacity of 116 mAh g^{-1} at 1 A g^{-1} and 100% capacity retention after 5000 cycles at a current density of 5 A g^{-1}.[13] Typically, V_2CT_x is known to exhibit intercalation capacitive behavior in neutral media with limited charge storage capacities. Due to recent advancements in the optimal synthesis strategies of V_2CT_x MXene and vanadium redox (electro)chemistry is being 'revisited' either through modification of electrode materials or through choice of electrolytes. However, water remains the major oxidant in transforming V_2CT_x MXene into its oxide form naturally, and limited chemical stability may pose a challenge in studying the intrinsic redox chemistry of vanadium carbide MXene.[9] In this work, we have employed a multilayered form of V_2CT_x MXene over delaminated, as the former is relatively stable compared to the latter. It is also interesting to look at the intrinsic electrochemistry of the composition at the multilayer stage, as there are no intercalants involved during chemical synthesis. Furthermore, to mitigate oxidation effects, a preintercalation strategy was employed during casting of the multilayer V_2CT_x MXene based electrodes. Room temperature ionic liquid was employed as a preintercalant and also as a surface protective layer to V_2CT_x MXene in casting the electrodes. Some of the

S. Yadav, N. Kurra
Department of Chemistry
Indian Institute of Technology Hyderabad
Kandi, Sangareddy, Telangana 502284, India
E-mail: narendra@chy.iith.ac.in

Supporting information for this article is available on the WWW under https://doi.org/10.1002/batt.202500305

Research Article
doi.org/10.1002/batt.202500305
Chemistry Europe
European Chemical Societies Publishing

chemical preintercalation strategies of V_2CT_x MXene were demonstrated with improved electrochemical performance to 98% capacity retention after 5000 cycles in a nonaqueous Li-ion electrolyte.[14] However, redox electrochemistry of V_2CT_x MXene in aqueous calcium electrolytes is underexplored. Moreover, the role of anion in influencing the charge storage capacity and solvent composition in affecting the cycling stability has not been reported hitherto.

We observed redox-type charge storage characteristics of preintercalated V_2CT_x MXene in calcium-ion-based electrolytes. A typical discharge capacity of 116 mAh g^{-1} was observed at a current density of 0.05 A g^{-1} in aqueous electrolytes, but inevitable capacity fading limits the long-term cycling stability. Therefore, a hybrid electrolyte, 1M calcium bis(trifluoromethanesulphonyl)imide [$Ca(TFSI)_2$] in propylene carbonate-water was employed to suppress the capacity degradation up to 30% while obtaining the specific capacity of 180 mAh g^{-1} at a current density of 0.09 A g^{-1} and an optimal potential window of operation. Hybrid electrolytes help in minimizing the activity of the water through hydrogen bonding, and hence, the reaction with the V_2CT_x MXene electrode is diminished.

2. Results and Discussion

The top-down wet chemical etching method was employed in synthesizing multilayered MXene from their respective MAX precursor.[15] Selective etching of Al atomic layer is based on relatively weaker bond strength of M—A compared to M—C bonds.[16] Vanadium carbide (V_2CT_x) MXene was synthesized by employing the mixed acid etching method (HF/HCl). The etchant solution consists of hydrofluoric acid (HF) and hydrochloric acid (HCl), which selectively etches the Al atomic layer from the V_2AlC MAX precursor (see experimental section). Presumably, the supporting acid, HCl, helps in dissolving etching by-products and is subsequently removed via washing and centrifugation.[17] The scanning electron microscopy (SEM) images of V_2AlC MAX phase and V_2CT_x MXene are shown in Figure S1a,b, Supporting Information. The structural characteristics of the V_2CT_x MXene were characterized by X-ray diffraction (XRD) as shown in Figure S1c, Supporting Information. The characteristic (002) peak in V_2AlC MAX phase at 2θ of 13.43° with a corresponding *d*-spacing of 6.59 Å has been downshifted to 7.39° (corresponding enlargement in *d*-spacing of 11.95 Å) in V_2CT_x MXene. The increase in *d*-spacing (5.36 Å) after the etching step involves the introduction of electronegative functional groups such as =O, —OH, —F, and —Cl at the expense of the removal of the Al atomic layer.

Figure 1a shows the strategy for deploying room-temperature ionic liquid (RTIL), 1-ethyl-3-methylimidazolium bis(trifluoromethanesulfonyl)imide (EMIM-TFSI), as a preintercalant during the MXene electrode fabrication process. Generally, 2D MXene layers tend to restack via weak van der Waals and hydrogen bonding interactions during the coating of electrodes, that may hamper electrolyte ion diffusion.[18] Preintercalation is one of the strategies for improving the electrochemical performance of 2D material-based electrodes.[19] Previous literature studies demonstrated the preintercalation of ionic liquid into

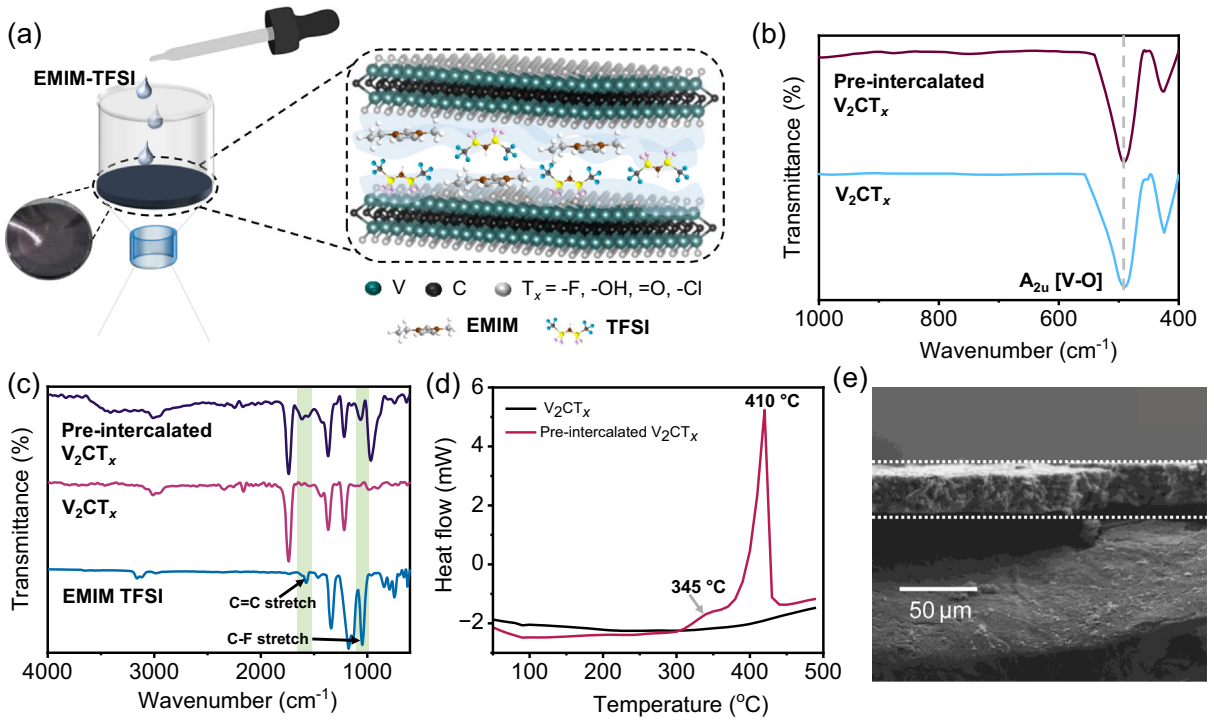

Figure 1. a) Schematic illustration depicting preintercalation of EMIM-TFSI ionic liquid into 2D galleries of V_2CT_x MXene. b) FTIR spectra of pristine and preintercalated V_2CT_x MXene. c) ATR-FTIR spectra of neat EMIM-TFSI, pristine, and preintercalated V_2CT_x MXene. d) DSC curves of preintercalated and pristine V_2CT_x MXene. e) Scanning electron micrograph of preintercalated V_2CT_x MXene coating on grafoil (cross-sectional view).

Research Article
doi.org/10.1002/batt.202500305
Chemistry Europe
European Chemical Societies Publishing

MXene galleries through immersion of free-standing $Ti_3C_2T_x$ films.[20,21] We adopted conventional electrode slurry preparation (refer to experimental section), which involves the introduction of ionic liquid (IL) to improve ionic accessibility between the MXene layers along with carbon black particles as nanoconduits for enhancing the electrical conductivity across the thickness of the electrode coating. Such kind of electrode coatings may be endorsed with facile diffusion of high charge density cations (in this case, Ca^{2+} ions) while providing access to redox-active sites. The typical preintercalation approach involves the addition of a few drops of RTIL, EMIM-TFSI, to the multilayered V_2CT_x MXene powder during vacuum-assisted filtration (shown in Figure 1a). Due to the low vapor pressure (40 nPa at 20 °C) of EMIM-TFSI, the loss of adsorbed/intercalated IL across V_2CT_x MXene is negligible (inset, Figure 1a). Such a preintercalation of MXene electrodes employing mineral salts in aqueous or organic solvents may lead to the precipitation of salt particles during the drying stage. It is known that the majority of the organic solvents or water undergo evaporation at a temperature of 200 °C, that eventually leads to the precipitation of salt particles throughout the volume of the electrode. Thus, a low vapor pressure ionic liquid remains the best choice in this case as a preintercalant. To ensure adequate soaking of EMIM-TFSI through adsorption sites/interlayer spaces of MXene coatings, samples were left in the desiccator for a few days.

Fourier transform infrared (FTIR) spectra showed the fingerprint region of V_2CT_x and preintercalated V_2CT_x MXene (Figure 1b). The intense peak at 490 cm^{-1} in V_2CT_x is due to the A_{2u} normal mode of vibration of V—O bond (V—O bending vibrations) and is in agreement with the reported literature.[22] The A_{2u}V—O peak remains unaffected after the preintercalation of the ionic liquid, signifying the preservance of the original bonding state. Attenuated total reflectance-FTIR (ATR-FTIR) spectra of neat EMIM-TFSI ionic liquid, preintercalated and pristine V_2CT_x MXene are shown in Figure 1c. The presence of signature peaks at 1574 and 1048 cm^{-1} corresponds to the C═C stretch of $EMIM^+$, and C—F stretch of $TFSI^-$, respectively. To further investigate the thermal characteristics of preintercalated ionic liquid, thermogravimetric analysis (TGA) was performed as shown in Figure S2, Supporting Information. In th case of V_2CT_x MXene, the onset of decomposition at 270 °C corresponds to the removal of surface functional groups and also chemisorbed structural water. However, in preintercalated V_2CT_x MXene, the onset of decomposition of EMIM-TFSI ionic liquid is observed at 400 °C, and the same can be seen in the TGA profile of preintercalated V_2CT_x MXene. Further differential scanning calorimetry (DSC) analysis was performed to provide insights into the thermal characteristics of pristine and preintercalated V_2CT_x MXene (Figure 1d). In V_2CT_x MXene, the stepwise decrease in the heat flow at low temperatures (100−300 °C) corresponds to the removal of chemisorbed water and surface functional groups, as shown in TGA curves. Moreover, in the case of preintercalated V_2CT_x MXene, an exothermic curve corresponds to the decomposition of EMIM-TFSI at a temperature of 410 °C, which corroborates well with the TGA data. Figure 1e shows the cross-sectional scanning electron micrograph of coating of the

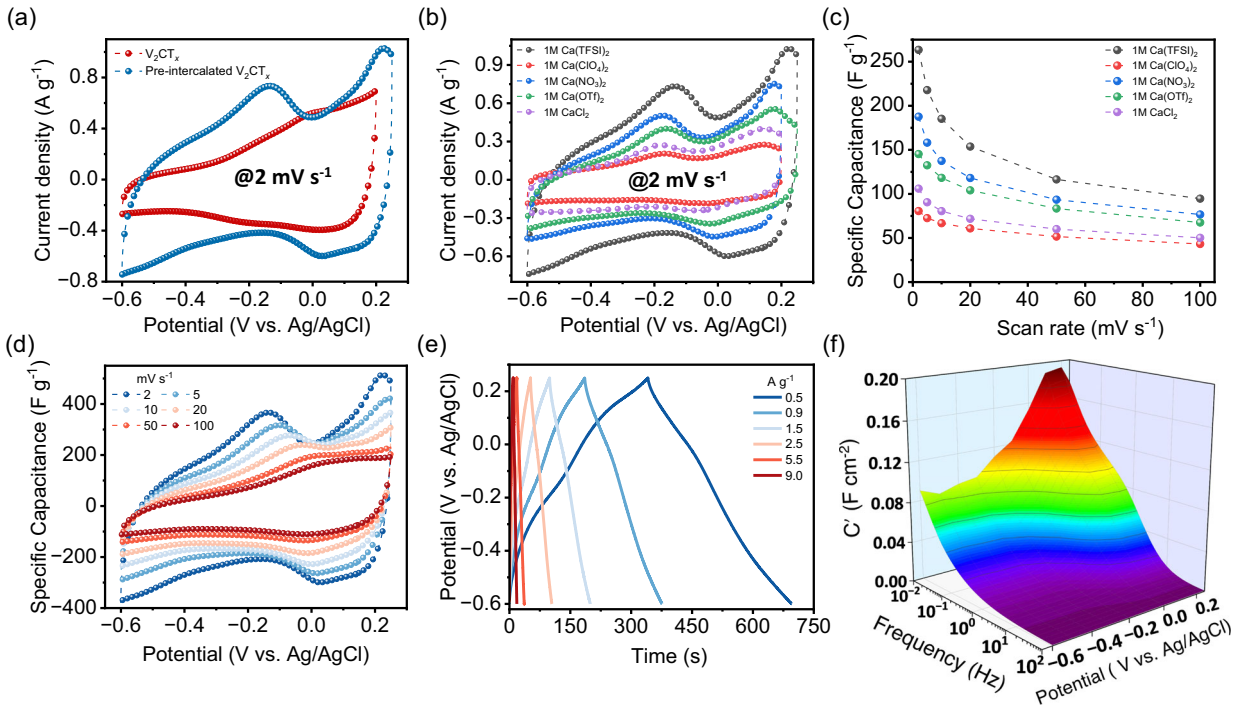

Figure 2. a) Cyclic voltammograms (CVs) of pristine V_2CT_x and preintercalated V_2CT_x MXene electrodes in 1M $Ca(TFSI)_2$ aqueous electrolyte at a scan rate of 2 mV s^{-1}. b) CVs at a scan rate of 2 mV s^{-1} and c) specific capacitance as a function of scan rate plot of preintercalated V_2CT_x MXene electrodes in various aqueous Ca-ion electrolytes. d) CVs of preintercalated V_2CT_x electrode in 1M $Ca(TFSI)_2$ electrolyte at various scan rates. e) Galvanostatic charge-discharge (GCD) profiles of preintercalated V_2CT_x electrode at different current densities. f) 3D Bode map of preintercalated V_2CT_x electrode in 1M $Ca(TFSI)_2$ electrolyte.

preintercalated V_2CT_x on grafoil current collector, depicting the uniform nature of the coating. XRD patterns of the pristine *ml*-V_2CT_x MXene and EMIM-TFSI preintercalated *ml*-V_2CT_x MXene electrode are shown in Figure S1d, Supporting Information.

It has been reported that MXenes exhibit proton-induced pseudocapacitive behavior in protic electrolytes while intercalation-induced capacitance in neutral aqueous electrolytes.[23] Typically, V_2CT_x MXenes are known to form EDLs via intercalated hydrated/solvated metal cations across interlayer spaces. To study the effect of anions on the charge storage behavior of V_2CT_x MXene, different calcium salts dissolved in deionized (DI) water were employed as electrolytes. The electrochemical performance of V_2CT_x MXene with and without preintercalation was compared in 1M calcium bis(trifluoromethanesulphonyl)imide [$Ca(TFSI)_2$] aqueous electrolyte. The cyclic voltammograms (CVs) of pristine and preintercalated V_2CT_x MXene at a scan rate of 2 mV s^{-1} are shown in **Figure 2**a. The CV curve of preintercalated V_2CT_x MXene exhibits two prominent anodic peaks at −0.13 V (vs. Ag/AgCl) and 0.22 V (vs. Ag/AgCl), and one broad cathodic peak at 0.03 V (vs. Ag/AgCl), signifies a redox-type of charge storage behavior. However, in the case of pristine V_2CT_x MXene, no redox signatures are observed in the operational potential window, indicating the formation of EDLs by the hydrated Ca^{2+} ions in the interlayer spaces. It was previously reported that the confined ionic liquid promotes the desolvation of Ca-ions and hence facilitates the partial charge transfer across the electrode–electrolyte interface.[24] The preintercalated V_2CT_x electrode showed a specific capacity of 80 mAh g^{-1}, that is two-fold superior to that of pristine V_2CT_x MXene (38 mAh g^{-1}) at a current density of 0.15 A g^{-1} in 1M $Ca(TFSI)_2$ aqueous electrolyte (Figure S3a, Supporting Information). Such a kind of improved Ca^{2+} ion charge storage capacity is attributed to the plausible interaction of desolvated Ca^{2+} ions with MXene surface terminal groups (typically oxy terminations) mediated via confined fluid, EMIM-TFSI.

Figure 2b compares CVs of preintercalated V_2CT_x MXene in different calcium-ion aqueous electrolytes such as 1M $Ca(TFSI)_2$, 1M $Ca(ClO_4)_2$, 1M $Ca(NO_3)_2$, 1M $Ca(OTf)_2$, and 1M $CaCl_2$ at a scan rate of 2 mV s^{-1}. The preintercalated V_2CT_x MXene showed a similar type of redox behavior, displaying two prominent anodic and one broad cathodic peak in aqueous Ca-ion based electrolytes. In the case of 1M $CaCl_2$ electrolyte, the CV curve resembles that of pristine V_2CT_x electrode, as shown in Figure 2a. Redox signatures of preintercalated V_2CT_x electrodes are prominent in the case of 1M $Ca(NO_3)_2$, 1M $Ca(OTf)_2$, and 1M $Ca(TFSI)_2$ aqueous electrolytes. However, the maximum capacitance value was observed in the case of 1M $Ca(TFSI)_2$ aqueous electrolyte. Due to the asymmetric nature of TFSI anion compared to the spherical type of chloride, perchlorate, and nitrate anions, $Ca(TFSI)_2$ may have relatively lower lattice enthalpy compared to other salts (Figure S4, Supporting Information).[25] Apparently, it turns out that Ca^{2+} interaction with the oxy terminations of V_2CT_x is facilitated in case of 1M $Ca(TFSI)_2$ electrolyte. As preintercalant has a common anion, that is, TFSI, Ca^{2+} ions have a greater tendency to get adsorbed/intercalated across V_2CT_x galleries unlike the case of other calcium salts. As a result, the preintercalated V_2CT_x MXene showed a specific capacitance of 263 F g^{-1} in 1M $Ca(TFSI)_2$ aqueous electrolyte (Figure 2c). The ionic conductivity values of 1M $Ca(TFSI)_2$, 1M $Ca(ClO_4)_2$, 1M $Ca(NO_3)_2$, 1M $Ca(OTf)_2$, and 1M $CaCl_2$ aqueous electrolytes are shown in Table S1, Supporting Information.

It was reported that V_2CT_x MXene showed pseudocapacitive behavior in acidic and basic electrolytes, giving rise to the typical capacitance of 380 F g^{-1}.[10] V_2CT_x MXene exhibited a specific capacitance of ≈225 F g^{-1} in 1M $MgSO_4$ electrolyte.[26] However, the preintercalation strategy enhanced capacitance by twofold in the case of high charge density Ca^{2+} cations when compared to pristine V_2CT_x electrodes. As shown in Figure 2d, redox peaks may not be prominent at high scan rates (>20 mV s^{-1}) due to capacitive type of adsorption of high charge density Ca^{2+} ions without charge transfer. Galvanostatic charge–discharge profiles appear to be quasi-triangular type across a range of current densities from 0.5 to 9.0 A g^{-1} (Figure 2e). Typical discharge times range from 360 s (corresponding current density of 0.5 A g^{-1}) to 10 s (corresponding current density of 9 A g^{-1}), which is characteristic discharge time scales of pseudocapacitive materials.[1]

To further investigate the kinetics of charge transfer across preintercalated and pristine V_2CT_x MXene electrodes by Ca^{2+} ions, electrochemical impedance spectra were analyzed. The presence of negligible semicircle in the Nyquist plot suggests low charge transfer resistance at the electrode–electrolyte interface in both electrodes with facile kinetics (Figure S3b, Supporting Information). However, equivalent series resistance (ESR) in preintercalated V_2CT_x MXene is 3 Ω, that is lower than pristine V_2CT_x MXene (ESR ≈5 Ω). This signifies that confined ionic liquid provides better ionic conductivity on top of adequate electronic conductivity of V_2CT_x MXene electrodes. Most importantly, confined fluidic layer acts like a nanolubricant in transporting the Ca-ions from one site to another site in the case of preintercalated electrodes at an ease. A 3D Bode plot of C′ as a function of frequency and potential was constructed to visualize the charge storage dynamics of preintercalated V_2CT_x MXene in 1M $Ca(TFSI)_2$ aqueous electrolyte. A maximum C′ value around 0.2 V (vs. Ag/AgCl) in the low-frequency region (<0.1 Hz), resembling that of a waterfall kind of appearance, indicating characteristic pseudocapacitive type of charge storage.[9]

The structural evolution of preintercalated V_2CT_x MXene upon (de)insertion of Ca^{2+} during charging and discharging was probed using in situ X-ray diffraction (XRD). The charge–discharge profile in **Figure 3**a shows the discharge starting from OCP (0.0 V vs. AC, labeled V_1) to −0.6 V vs. AC (labeled V_7), followed by charging up to V_{15} (0.2 V vs. AC), and subsequent discharge to −0.2 V vs. AC (labeled V_{19}). Figure 3b displays the XRD patterns recorded at different charge–discharge potentials, showing the (002) peak at 2θ ≈8.9°, which remains unchanged as a funtion of potentials and maintains a *d*-spacing of 10.0 Å. However, the emergence of low-indexed reflection at 7.2° corresponds to expanded interlayer spacing (0.2 Å)(Figure 3c). Such kind of sudden appearance of additional reflections at low 2θ angles corresponds to the insertion of large size hydrated water complexes, causing expansion of the layers. Due to the hydrophilic nature of V_2CT_x MXene galleries, spontaneous intercalation of water molecules causes the enlargement in the *d*-spacing. Such behavior is

Research Article
doi.org/10.1002/batt.202500305
Chemistry Europe
European Chemical Societies Publishing

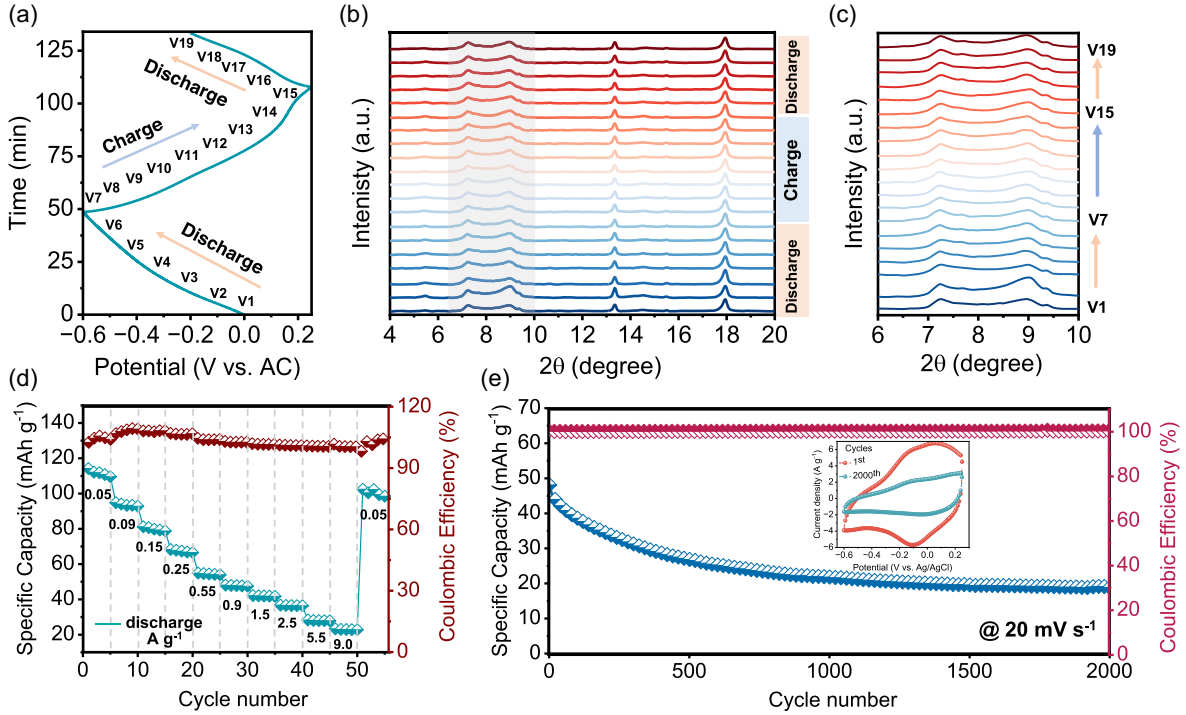

Figure 3. a) GCD profiles of preintercalated V_2CT_x MXene in 1M $Ca(TFSI)_2$ aqueous electrolyte during in situ XRD measurements. b) In situ XRD patterns of preintercalated V_2CT_x MXene at various charging-discharging potentials (discharging: OCP to −0.6 V (vs. AC), charging: −0.6 to 0.2 V (vs. AC) in 1M $Ca(TFSI)_2$ aqueous electrolyte. c) Enlarged view of (002) peak, showing no change in the *d*-spacing value during the charge–discharge cycle. d) Rate performance and e) cycling stability of preintercalated V_2CT_x MXene in 1M $Ca(TFSI)_2$ aqueous electrolyte, and CVs of 1st and 2000th cycle shown in the inset.

demonstrated by Houdeville et al. in the case of lithium intercalation into TiS_2 electrodes with and without PC solvent, where only in the former case, a new cointercalation phase was formed and identified by the appearance of new (00*l*) cosignals (where $l = 1, 2, 3$).[27] Cointercalation reactions were also observed in $Ti_3C_2T_x$ MXenes, and the change of interlayer space was governed by the size of the ion-solvent complex. Hydrated Li-ions showed an enlarged shift in the (002) peak compared to solvated Li-ions (acetonitrile and DMSO).[28,29] However, there was no shift in the (002) peak when propylene carbonate was employed as a solvent for Li-TFSI salt.

Figure 3d shows the rate performance of preintercalated V_2CT_x MXene in 1 M $Ca(TFSI)_2$ aqueous electrolyte at various current densities (0.05 to 9 A g^{-1}). V_2CT_x MXene shows an average reversible capacity of 116 mAh g^{-1} at a current density of 0.05 A g^{-1}. As the current density increases to 9 A g^{-1}, the average discharge capacity delivered by the electrode is 23 mAh g^{-1}. Pristine V_2CT_x MXene shows an average reversible capacity of 38 mAh g^{-1} at a current density of 0.15 A g^{-1}. As the rate increases to 7 A g^{-1}, 18% capacity retention (7 mAh g^{-1}) was observed with 100% Coulombic efficiency (Figure S5, Supporting Information). In contrast, the preintercalated V_2CT_x MXene electrode exhibits a specific capacity of 80 mAh g^{-1} at 0.15 A g^{-1}, which is 2 times higher than that of pristine electrode, and retains 30% of its capacity when the rate increases to 9 A g^{-1}. Further, when the current density changes from 9 to 0.05 A g^{-1}, the discharging capacity recovers to 90% of its initial capacity (103 mAh g^{-1}) with 100% Coulombic efficiency. The longstanding cyclic stability of the preintercalated V_2CT_x MXene was tested for 2000 cycles at a constant scan rate of 20 mV s^{-1} (Figure 3e). At initial cycles, the discharge capacity is about 45 mAh g^{-1}, and after continuous 2000 cycles, a capacity retention of ≈40% was observed with 100% Coulombic efficiency. Such a capacity fading can be attributed to the chemical dissolution of V_2CT_x electrodes in aqueous media.[9]

Further, the electrochemical performance of preintercalated V_2CT_x MXene was also investigated in 1M $Ca(TFSI)_2$ hybrid (PC: H_2O in 2:1 and 1:2 volume) electrolyte. **Figure 4**a shows the ATR-FTIR spectra of 1M $Ca(TFSI)_2$ electrolyte in aqueous (H_2O), organic (PC), and hybrid (PC: H_2O) solvents. In the FTIR spectra, the -OH stretching region (≈3000–3600 cm^{-1}) shows notable changes when moving from an aqueous to an organic electrolyte. In aqueous systems, a broad and intense band is observed that is characteristic of strong intermolecular hydrogen bonding between water molecules, whereas the band intensity is reduced in organic electrolyte. Upon mixing PC solvent to form a hybrid electrolyte, this band typically narrows and shifts to a higher wavenumber, indicating weaker H-bonding (water–organic interactions). As PC is polar and is highly miscible with water, with a dielectric constant of 64.92 (donor number of 15.1 kcal mol^{-1}), PC is known to reduce the solvating power of water in the case of multivalent ions such as Ca^{2+} ions.[30,31] Similarly, the intense peak at 1300–1380 cm^{-1} corresponds to asymmetric stretching vibrations of SO_2 in TFSI anions.[32] In organic electrolyte, the SO_2 peaks remain unaltered due to low ion-ion interactions.

Figure 4b shows the comparative CVs of preintercalated V_2CT_x MXene in 1M $Ca(TFSI)_2$ dissolved in H_2O, PC, and PC: H_2O (2:1) solvents at a scan rate of 2 mV s^{-1}. The potential window got

Research Article
doi.org/10.1002/batt.202500305

Chemistry Europe
European Chemical Societies Publishing

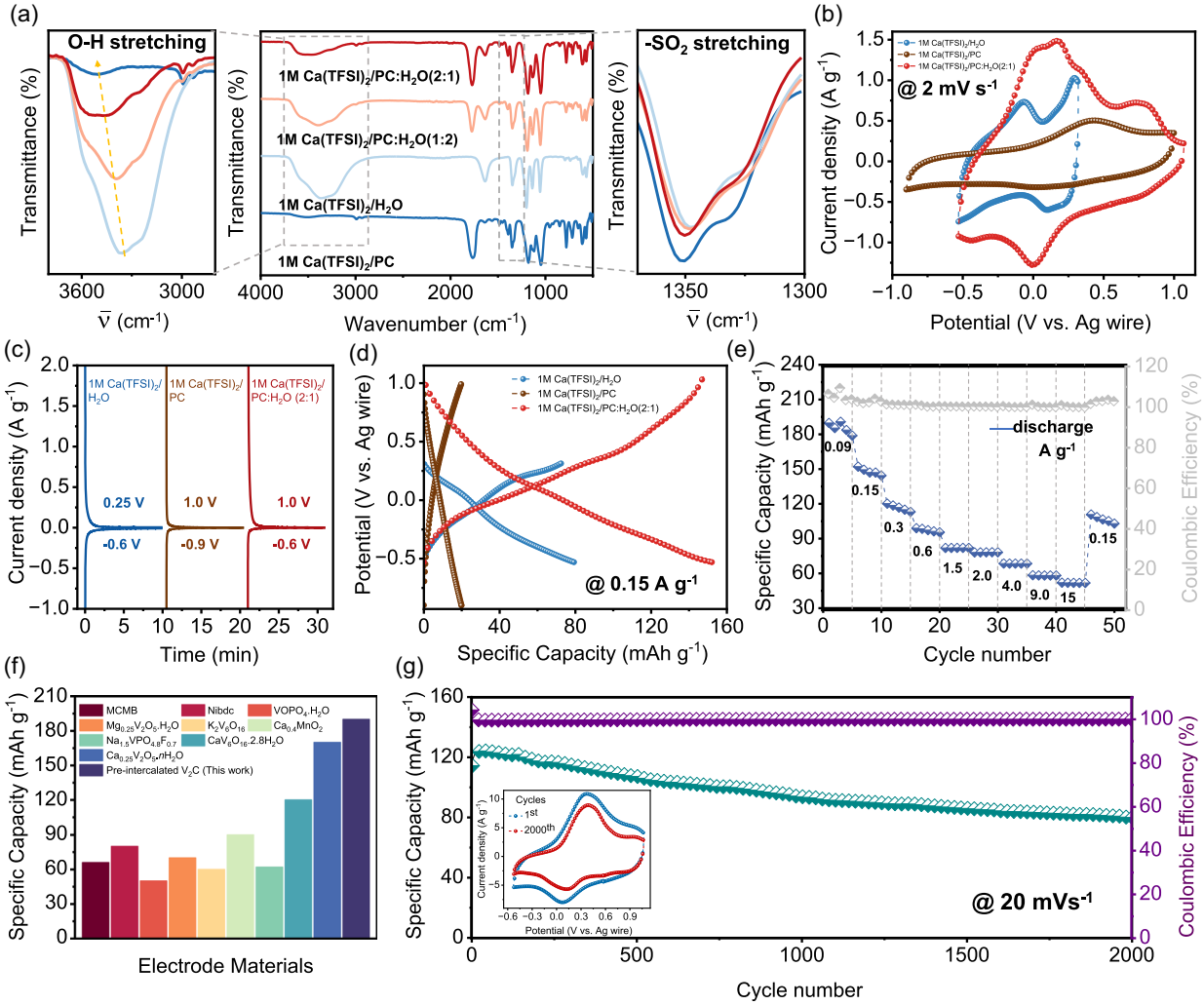

Figure 4. a) ATR-FTIR spectra of 1M $Ca(TFSI)_2$ electrolyte in propylene carbonate (PC, blue), water (H_2O, turquoise), and hybrid- PC: H_2O (1:2-orange, 2:1-red) solvents, insets showing the —OH stretching and —SO_2 asymmetric stretching regions. b) CVs of preintercalated V_2CT_x MXene in 1M $Ca(TFSI)_2$ electrolyte in PC, H_2O, and PC: H_2O (2:1) solvents at a scan rate of 2 mV s^{-1}. c) Chronoamperometry of preintercalated V_2CT_x MXene in 1M $Ca(TFSI)_2$ electrolyte in PC, H_2O, and PC: H_2O (2:1) solvents. d) GCD profiles of preintercalated V_2CT_x MXene in 1M $Ca(TFSI)_2$ electrolyte in PC, H_2O, and PC: H_2O (2:1) solvents at a current density of 0.15 A g^{-1}. e) Rate performance of preintercalated V_2CT_x MXene in 1M $Ca(TFSI)_2$ hybrid electrolyte (PC: H2O-2:1) at different current densities. f) Histogram showing the reversible calciation capacity of preintercalated V_2CT_x MXene with other reported electrode materials at a current density of 0.1 A g^{-1}. g) Cycling performance of preintercalated V_2CT_x MXene in 1M $Ca(TFSI)_2$ electrolyte in PC: H_2O (2:1) solvent at a scan rate of 20 mV s^{-1}, inset showing the CVs of 1st and 2000th cycle.

enhanced in the hybrid electrolyte compared to aqueous due to suppression of anodic oxidation of V_2CT_x MXene by the addition of organic electrolyte. To determine the stable electrochemical window of the V_2CT_x electrode in $Ca(TFSI)_2$ electrolytes in different solvents, chronoamperometry tests were conducted (Figure 4c). The results revealed steady-state leakage currents below 0.1 A g^{-1} between −0.6 V to 0.25 V (vs. Ag/AgCl) in case of aqueous electrolyte and −0.9 to 1 V (vs. Ag wire) in organic electrolyte. However, in the hybrid electrolyte, the window extended up to 1 V (vs. Ag/AgCl) by suppressing the anodic oxidation of V_2CT_x MXene. The preintercalated V_2CT_x MXene shows two broad anodic peaks at 0.1 and 0.7 V (vs. Ag/AgCl), shown in Figure 4b (red color). Preintercalated V_2CT_x MXene outperforms in the hybrid electrolyte compared to aqueous (Figure 2d) and organic (Figure S6, Supporting Information) electrolytes, showing a specific capacity of 150 mAh g^{-1} at a current density of 0.15 A g^{-1} (Figure S7, Supporting Information), which is almost two times higher than aqueous and seven times higher than organic electrolyte (Figure 4d).

The rate performance of preintercalated V_2CT_x MXene in 1M $Ca(TFSI)_2$ hybrid electrolyte (PC: H_2O-2:1) is shown in Figure 4e. The reversible calciation capacity shown by the electrode is 180 m Ah g^{-1} at 0.09 A g^{-1} and retains 150, 115, 97, 82, 78, 68, 58, and 52 mAh g^{-1} at current densities of 0.15, 0.3, 0.6, 1.5, 2, 4, 9, and 15 A g^{-1} respectively. The electrochemical performance of preintercalated V_2CT_x MXene in the aqueous hybrid electrolyte is superior to other reported electrode materials for calcium-ion storage (Figure 4f). The preintercalated V_2CT_x MXene shows 2.5 times higher calciation capacity than that of mesocarbon microbeads (MCMB, 66 mAh g^{-1})[33] and 1.5 times higher than CaV_6O_{16}·2.8H_2O (120 mAh g^{-1}).[34] Similarly, other materials such as $Ca_{0.4}MnO_2$,[35] $Mg_{0.25}V_2O_5$·H_2O,[36] $K_2V_6O_{16}$,[37] $Na_{1.5}VPO_{4.8}F_{0.7}$,[38]

$VOPO_4{\cdot}H_2O$,[39] and $Ca_{0.25}V_2O_5{\cdot}nH_2O$[40] shows reversible calciation capacity of 90, 60, 60, 62, 50, and 170 mAh g^{-1},respectively. Figure 4g shows the cycling performance of preintercalated V_2CT_x MXene in a hybrid 1M $Ca(TFSI)_2$ electrolyte. The electrode exhibited outstanding capacity retention, maintaining 70% of its initial storage capability after completing 2000 charge/discharge cycles at a scan rate of 20 mV s^{-1}. The introduction of hybrid solvents significantly improved cycling stability, and 70% capacity retention was observed after 2000 cycles, unlike the case of aqueous electrolyte (retention is 38% only). This reduction in the capacity fading in hybrid solvents reduces degradation of V_2CT_x electrode with long-term cycling stability. Systematic studies need to be performed to understand the impact of metal dissolution or chemical instability related to carbon vacancies of vanadium carbide MXene on the cycling life by employing inductively coupled plasma-optical emission spectroscopy techniques.[41] This study opens avenues for the exploration of hybrid electrolytes for the improved cycling stability and optimal electrochemical performance of the M_2C MXene compositions.

3. Conclusion

Ionic liquid preintercalated V_2CT_x MXene electrodes showed redox charge storage characteristics in calcium-ion electrolytes. Asymmetry in the anion structure promoted Ca^{2+} interaction with the surface terminations, with partial charge transfer mediated through confined 1-ethyl-3-methylimidazolium bis(trifluoromethylsulfonyl) imide (EMIM-TFSI) fluidic layer. Despite typical calciation charge storage capacities beyond 100 mAh g^{-1} in aqueous electrolytes, inevitable capacity fading resulted in the long-term instability. A hybrid electrolyte combining propylene carbonate and water showed an optimal electrochemical performance of 150 mAh g^{-1} at a current density of 0.15 A g^{-1} with an enlarged potential window of 1.6 V and capacity retention of 70% over 2000 cycles. The role of intermolecular hydrogen bonding interactions in influencing the electrochemical performance of V_2CT_x MXene electrodes was investigated by employing Fourier transform infrared (FTIR) spectroscopy . This study opens avenues for the development of hybrid electrolytes for the improved electrochemical performance of MXene compositions.

4. Experimental Section

All chemicals were used as received, without further purification. Layered ternary carbide V_2AlC (MAX phase, 32 μm particle size) was procured from Y-carbon, Ukraine Ltd.

Synthesis of Multilayered V_2CT_x MXene

Multilayered V_2CT_x (*ml*-V_2CT_x) MXene was synthesized from its V_2AlC MAX precursor (32 microns, Carbon Ukraine Ltd.) by the wet chemical etching method. A solution consisting of 12 mL of 40 wt% hydrofluoric acid (HF, Acros Organics) and 8 mL of 12 M hydrochloric acid (HCl, Fisher Chemical) was employed to selectively etch 'Al' atomic layer from the V_2AlC MAX phase. The etchant solution was taken in a high-density polyethylene bottle, and 1 g of V_2AlC ceramic powder was slowly added to the solution under constant stirring at 150 rpm. Due to the exothermic nature of the etching reaction, the reaction mixture was kept in an ice bath (0 °C) to avoid the oxidation/dissolution of the V_2AlC MAX phase at the initial stages of the etching reaction. Once the bubbling stopped, the reaction mixture was transferred to an oil bath held at 50 °C and was stirred at 400 rpm for 80 h. The multilayered V_2CT_x MXene obtained was washed repeatedly with deionized water via centrifugation at 3500 rpm for 5 min to remove the residual acid present. The resultant light green supernatant obtained in the initial washing cycles was decanted. Washing was continued until a pH of ≈6 was obtained. Typically, 1 to 1.5 L of DI water was employed for washing the acidic etchants to obtain the *ml*-V_2CT_x MXene in neutral aqueous medium.

Fabrication of Preintercalated V_2CT_x MXene Electrode

The *ml*-V_2CT_x MXene dispersed in DI water was filtered by vacuum-assisted filtration to remove the water. Celgard (pore size, 60 nm) was used as the porous membrane, which helps in retaining the solid particles while passing water through the membrane. To the resultant V_2CT_x sediment, a few drops of propylene carbonate (PC, Sigma Aldrich) were added, which possibly replaced the water molecules trapped between the V_2CT_x MXene layers. Thus, the obtained wet cake type V_2CT_x MXene was soaked in 0.3 mL of neat 1-ethyl-3-methylimidazolium bis(trifluoromethylsulfonyl) imide (EMIM-TFSI, TCI) ionic liquid (IL). To enable preintercalation, ionic liquid-soaked V_2CT_x MXene was transferred to a desiccator and kept at room temperature for a few days (at least 72 h). The ionic liquid preintercalated V_2CT_x MXene was transferred to a vacuum oven and kept at 200 °C overnight. The vacuum drying was done at 200 °C to eliminate PC and trapped residual water molecules. Due to the low vapor pressure and nonvolatile nature of EMIM-TFSI, it remains within the V_2CT_x MXene, possibly occupying the defective sites as well as interlayer spaces.

To fabricate preintercalated V_2CT_x electrodes, a homogeneous, thick slurry was made by grinding ionic liquid preintercalated V_2CT_x MXene (80 wt%), carbon black (Super P C645, 10 wt%, Timical), and polyvinylidene fluoride (PVDF) binder (10 wt%, Sigma–Aldrich) in a mortar and pestle. During grinding, N-methyl-2-pyrrolodine (NMP) was added in minimal amounts for proper mixing of the binder and additive components with V_2CT_x MXene. The homogeneous wet slurry was coated onto the graphite foil via a doctor blade coater. The graphite foils coated with slurry were vacuum dried overnight at 70 °C and then calendered (LKS-CM100, Labkarts) to ensure a strong connection between the electrode material and the current collector. 3 mm diameter electrodes were punched out from the material-coated graphite foil with a mass loading of 1.4 mg cm^{-2}.

Preparation of Activated Carbon (AC) Film

For the preparation of activated carbon films, 95 wt% of activated carbon (YP50F, Kuraray, Japan) and 5 wt% of polytetrafluoroethylene (60 wt% in water, Sigma Aldrich) were ground homogeneously using a mortar and pestle by adding small amounts of ethanol. This blended mixture was then rolled into a ≈100 μm thick film. The film was vacuum dried for 12 h at a temperature of 70 °C.

Material Characterization

The powder X-ray diffractometer (Malvern PANalytical, UK) was used to record the XRD patterns. It was equipped with a CuK_α (1.5406 Å) radiation source; the step size and the dwell time were 0.013° and 0.13 s, respectively. The current and tension were maintained at 40 mA and 40 kV, respectively. SEM (JEOL JIB4700F) was used to image the morphology of V_2AlC MAX and *ml*-V_2CT_x MXene. ATR-FTIR, Alpha, Bruker) equipped with a diamond crystal was utilized to record FTIR spectra

and investigate the presence of EMIM-TFSI ionic liquid in the V_2CT_x MXene. ATR-FTIR spectra were recorded in the range of 500–4000 cm^{-1} at a resolution of 4 cm^{-1}. To investigate the effect of preintercalation on the fingerprint region of V_2CT_x, infrared spectra were recorded for pristine and preintercalated V_2CT_x MXene in a Jasco FTIR-4600 spectrometer in the range of 400–4000 cm^{-1} at a resolution of 4 cm^{-1}, using a KBr pellet. Thermal analyzer SDT Q600 (TA Instruments Pvt. Ltd., USA) was utilized for TGA at a heating rate of 10 °C min^{-1} from room temperature to 900 °C under an argon atmosphere with a constant gas flow of 100 m min^{-1} in an Al-type crucible. Further, DSC Q200 (TA Instruments Pvt. Ltd., USA) was used for thermal characterization of pristine and preintercalated V_2CT_x MXene using constant N_2 gas flow at 50 m min^{-1} with a heating rate of 10 °C min^{-1} from room temperature to 500 °C. The structural evolution of the working electrodes during discharging/charging cycles was studied using in situ XRD. A powder X-ray diffractometer (Malvern PANalytical, UK), with CuK_α (1.5406 Å) radiation source, was utilized for recording the in situ XRD patterns from 4° to 12° (2θ values).

Electrochemical Measurements

SP-150e electrochemical workstation (BioLogic, France) was used to perform electrochemical measurements such as cyclic voltammetry, galvanostatic charge–discharge (GCD), chronoamperometry, and electrochemical impedance spectroscopy (EIS) at room temperature in three-electrode Swagelok cells. The electrochemical setup consists of V_2CT_x and preintercalated V_2CT_x MXene as the working electrodes, and activated carbon and Ag/AgCl were used as counter and reference electrodes, respectively. The glass microfiber membrane (Whatman) was used as a separator.

Typically, an Ag/AgCl reference electrode is used to study the electrochemical performance in aqueous systems, whereas in nonaqueous systems (such as propylene carbonate, PC), a silver wire is employed as a quasi-reference electrode. The potential of Ag wire with respect to Ag/AgCl was calibrated through employing an internal standard of ferrocene/ferrocenium redox couple, and it is found to be

$$E_{\text{Ag wire}}(V) = E_{\text{Ag/AgCl}}(V) + 0.07\,\text{V} \quad (1)$$

The electrochemical performance of V_2CT_x MXene electrodes was investigated in a variety of aqueous electrolytes such as 1M calcium bis(trifluoromethanesulphonyl)imide [$Ca(TFSI)_2$, TCI], 1M calcium perchlorate tetrahydrate [$Ca(ClO_4)_2.4H_2O$, Sigma Aldrich], 1M calcium nitrate tetrahydrate [$Ca(NO_3)_2.4H_2O$, Sigma Aldrich], 1M Calcium trifluoromethane sulfonate [$Ca(OTf)_2$, TCI] and 1M calcium chloride [$CaCl_2$, Sigma Aldrich]. CVs were recorded at different scan rates, ranging from 1 to 100 mV s^{-1}. GCD profiles were recorded by applying different current densities in the range of 0.05 to 9 A g^{-1}. The charge transfer and mass transfer kinetics were investigated across V_2CT_x MXene-electrochemical interfaces by employing staircase potentio-EIS. In this technique, different DC potentials were applied from 0.25 to −0.60 V (vs. Ag/AgCl), and the potential of the working electrode was held for 10 min. Typically, a sinusoidal voltage with an amplitude of 10 mV was imposed on top of direct current (dc) applied potentials on the working electrodes in the frequency range of 100 kHz – 10 mHz.

Specific capacity was calculated by integrating the current versus time plots.

$$\text{Specific capacity} = \frac{1}{m}\int idt \quad (2)$$

The real capacitance, C' and imaginary capacitance, C'' were calculated by using the following equations

$$C' = -Z''/2\pi f|Z|^2 \quad (3)$$

$$C' = -Z'/2\pi f|Z|^2 \quad (4)$$

where $|Z|$ is the absolute value of the impedance (Ω), Z' and Z'' are the real component and the imaginary components of impedance, respectively, and f is the frequency (Hz).

The structural evolution of the working electrodes during discharging/charging cycles was studied using in situ XRD. A powder X-ray diffractometer equipped with CuK_α (1.5406 Å) radiation source was utilized for recording the in situ XRD patterns from 4° to 12° (2θ values). A CR2032 coin cell with a hole of 8 mm diameter at the positive terminal was used. An over-capacitive activated carbon and glass microfiber (Whatman) membranes were used as counter electrodes and separators, respectively. During in situ XRD, a portable SP-150e electrochemical workstation (BioLogic, France) was utilized to apply the desired potentials to the working electrodes.

Acknowledgements

S.Y. acknowledges the scholarship support from PMRF, India. N.K. acknowledges support from the Indian Institute of Technology Hyderabad, India, and Science and Engineering Research Board, India for financial support (CRG/2021/001094).

Conflict of Interest

The authors declare no conflict of interest.

Data Availability Statement

The data that support the findings of this study are available from the corresponding author upon reasonable request.

Keywords: 2D charge hosts · hybrid Ca-ion electrolytes · preintercalations · pseudocapacitance · v_2c MXene

[1] S. Fleischmann, J. B. Mitchell, R. Wang, C. Zhan, D. Jiang, V. Presser, V. Augustyn, *Chem. Rev.* **2020**, *120*, 6738.
[2] X. Li, Z. Huang, C. E. Shuck, G. Liang, Y. Gogotsi, C. Zhi, *Nat. Rev. Chem.* **2022**, *6*, 389.
[3] A. Vahid Mohammadi, J. Rosen, Y. Gogotsi, *Science* **2021**, *372*, eabf1581.
[4] B. Anasori, M. R. Lukatskaya, Y. Gogotsi, *Nat. Rev. Mater.* **2017**, *2*, 16098.
[5] M. Okubo, A. Sugahara, S. Kajiyama, A. Yamada, *Acc. Chem. Res.* **2018**, *51*, 591.
[6] S. Yadav, N. Kurra, *Energy Storage Mater.* **2024**, *65*, 103094.
[7] N. Kurra, S. Uzun, G. Valurouthu, Y. Gogotsi, *Energy Storage Mater.* **2021**, *39*, 347.
[8] I. Hussain, O. J. Kewate, A. Hanan, F. Bibi, M. S. Javed, P. Rosaiah, M. Ahmad, X. Chen, I. Shaheen, M. B. Hanif, A. H. Bhatti, M. A. Assiri, W. A. Zoubi, K. Zhang, *ChemSusChem* **2024**, *17*, e202400283.
[9] K. Matthews, T. Zhang, C. E. Shuck, *Chem. Mater.* **2022**, *34*, 499.
[10] T. Zhang, K. Matthews, *ACS Energy Lett.* **2022**, *7*, 3864.
[11] Y. Dall'Agnese, P.-L. Taberna, Y. Gogotsi, P. Simon, *J. Phys. Chem. Lett.* **2015**, *6*, 2305.
[12] A. Vahid Mohammadi, A. Hadjikhani, S. Shahbazmohamadi, M. Beidaghi, *ACS Nano* **2017**, *11*,11135.
[13] Z. Bao, C. Lu, Q. Liu, F. Ye, W. Li, Y. Zhou, L. Pan, L. Duan, H. Tang, Y. Wu, L. Hu, Z. Sun, *Nat. Commun.* **2024**, *15*, 1934.
[14] F. Liu, Y. Liu, X. Zhao, K. Liu, H. Yin, L.-Z. Fan, *Small* **2020**, *16*, 1906076.
[15] Y. Gogotsi, *MXenes: from Discovery to Applications of Two-Dimensional Metal Varbides and Nitrides*, Jenny Stanford Publishing, Singapore, **2023**.

[16] B. C. Wyatt, A. Rosenkranz, B. Anasori, *Adv. Mater.* **2021**, *33*, 2007973.
[17] M. Seredych, C. E. Shuck, D. Pinto, M. Alhabeb, E. Precetti, G. Deysher, B. Anasori, N. Kurra, Y. Gogotsi, *Chem. Mater.* **2021**, *31*, 3324.
[18] Y. Xia, T. S. Mathis, M.-Q. Zhao, B. Anasori, A. Dang, Z. Zhou, H. Cho, Y. Gogotsi, S. Yang, *Nature* **2018**, *557*, 409.
[19] X. Yao, Y. Zhao, F. A. Castro, L. Mai, *ACS Energy Lett.* **2019**, *4*, 771.
[20] Z. Lin, D. Barbara, P.-L. Taberna, K. L. Van Aken, B. Anasori, Y. Gogotsi, P. Simon, *J. Power Sources* **2016**, *326*, 575.
[21] Z. Lin, P. Rozier, B. Duployer, P.-L. Taberna, B. Anasori, Y. Gogotsi, P. Simon, *Electrochem. Commun.* **2016**, *72*, 50.
[22] T. Parker, D. Zhang, D. Bugallo, K. Shevchuk, M. Downes, G. Valurouthu, A. Inman, B. Chacon, T. Zhang, C. E. Shuck, Y.-J. Hu, Y. Gogotsi, *Chem. Mater.* **2024**, *36*, 8437.
[23] Y. Ando, M. Okubo, A. Yamada, M. Otani, *Adv. Funct. Mater.* **2020**, *30*, 2000820.
[24] S. Yadav, N. Kurra, *J. Mater. Chem. A* **2024**, *12*, 32182.
[25] J. D. Forero-Saboya, E. Marchante, R. B. Araujo, D. Monti, P. Johansson, A. Ponrouch, *J. Phys. Chem. C* **2019**, *123*, 29524.
[26] Q. Shan, X. Mu, M. Alhabeb, C. E. Shuck, D. Pang, X. Zhao, X.-F. Chu, Y. Wei, F. Du, G. Chen, Y. Gogotsi, Y. Gao, Y. Dall'Agnese, *Electrochem. Commun.* **2018**, *96*, 103.
[27] R. G. Houdeville, A. P. Black, A. Ponrouch, M. R. Palacín, F. Fauth, *J. Electrochem. Soc.* **2021**, *168*, 030514.
[28] X. Wang, T. S. Mathis, Y. Sun, W. Y. Tsai, N. Shpigel, H. Shao, D. Zhang, K. Hantanasirisakul, F. Malchik, N. Balke, D. E. Jiang, P. Simon, Y. Gogotsi, *ACS Nano* **2021**, *15*, 15274.
[29] X. Wang, T. S. Mathis, K. Li, Z. Lin, L. Vlcek, T. Torita, N. C. Osti, C. Hatter, P. Urbankowski, A. Sarycheva, M. Tyagi, E. Mamontov, P. Simon, Y. Gogotsi, *Nat. Energy* **2019**, *4*, 241.
[30] H. Zhang, L. Qiao, H. Kühnle, E. Figgemeier, M. Armand, G. G. Eshetu, *Energy Environ. Sci.* **2023**, *16*, 11.
[31] A. Ponrouch, C. Frontera, F. Bardé, M. R. Palacín, *Nat. Mater.* **2016**, *15*, 169.
[32] J. Wang, R. Yu, Y. Jiang, F. Qiao, X. Liao, J. Wang, M. Huang, F. Xiong, L. Cui, Y. Dai, L. Zhang, Q. An, G. He, L. Mai, *Energy Environ. Sci.* **2024**, *17*, 6616.
[33] S. Wu, F. Zhang, Y. Tang, *Adv. Sci.* **2018**, *5*, 1701082.
[34] J. Wang, J. Wang, Y. Jiang, F. Xiong, S. Tan, F. Qiao, J. Chen, Q. An, L. Mai, *Adv. Funct. Mater.* **2022**, *32*, 2113030.
[35] X. Tang, D. Zhou, B. Zhang, S. Wang, P. Li, H. Liu, X. Guo, P. Jaumaux, X. Gao, Y. Fu, C. Wang, C. Wang, G. Wang, *Nat. Commun.* **2021**, *12*, 2857.
[36] X. Xu, M. Duan, Y. Yue, Q. Li, X. Zhang, L. Wu, P. Wu, B. Song, L. Mai, *ACS Energy Lett.* **2019**, *4*, 1328.
[37] L.-W. Dong, R.-G. Xu, P.-P. Wang, S.-C. Sun, Y. Li, L. Zhen, C.-Y. Xu, *J. Power Sources* **2020**, *479*, 228793.
[38] Z.-L. Xu, J. Park, J. Wang, H. Moon, G. Yoon, J. Lim, Y.-J. Ko, S.-P. Cho, S.-Y. Lee, K. Kang, *Nat. Commun.* **2021**, *12*, 3369.
[39] J. Wang, S. Tan, F. Xiong, R. Yu, P. Wu, L. Cui, Q. An, *Chem. Commun.* **2020**, *56*, 3805.
[40] X. Qin, X. Zhao, G. Zhang, Z. Wei, L. Li, X. Wang, C. Zhi, H. Li, C. Han, B. Li, *ACS Nano* **2023**, *17*, 12040.
[41] Z. Zhao, W. Zhang, D. Wang, L. Li, Q. Liang, W. Li, C. Lu, S. Jo Yoo, J.-G. Kim, Z. Chen, Y. Li, X. Zou, F. Liu, X. Zhou, K. Song, J. Li, W. Zheng, *Angew. Chem. Int. Ed.* **2024**, *63*, e202414420.

Manuscript received: April 23, 2025
Revised manuscript received: June 28, 2025
Version of record online: